Geometric Electric Dipole Moments and CP Violation in the MMA–DMF Framework

Paulo Jorge Adriano *

Posted Date: 26 December 2025

doi: 10.20944/preprints202512.2427.v1

Keywords: electric dipole moment; CP violation; geometric screening; density–time scaling; matched filtering; GNOME; laboratory replication; Jordan-frame coupling

 doi:10.20944/preprints202512.2427.v1

Article

Geometric Electric Dipole Moments and CP Violation in the MMA–DMF Framework

Paulo Adriano

Independent Researcher, Portugal; home@chiptec.net

Abstract

We present a consolidated, test-driven account of geometric electric dipole moments (EDMs) and CP violation within the MMA-DMF framework, compiled from the December 2025 audit archive and its Gold/Platinum/Diamond validation artifacts. The central claim is operational: CP violation is dynamically active during the electroweak window ($\dot{\phi} \neq 0$) but becomes effectively static and screened at late times ($\dot{\phi} \to 0$), so present-day EDM searches must target transient spectra rather than only DC offsets. Crucially, the operational kernel is *rigid and degree-of-freedom-free*: the analysis is executed with a fixed "Golden" parameter set (no tunable degrees of freedom in the pipeline), and all detection statements are framed as falsifiable pass/fail criteria. We show how the density–time scaling law $\tau(\rho_{\mathrm{env}})$ induces a mandatory downward-chirp "Sad Trombone" transient, and we specify a matched-filter protocol with density-aware templates. We also provide a laboratory handoff for the *T-Environment* density-swap experiment, including hardware requirements, timing constraints, logging schema, and acceptance criteria needed for an independent replication campaign.

Keywords: electric dipole moment; CP violation; geometric screening; density–time scaling; matched filtering; GNOME; laboratory replication; Jordan-frame coupling

---

1. Introduction

The empirical absence of permanent electric dipole moments at current sensitivity places severe constraints on CP-violating physics beyond the Standard Model. At the same time, cosmology requires CP violation in the early universe to explain the baryon asymmetry. This tension is especially acute for the strong CP problem: the effective QCD vacuum angle must be extremely small today, yet conventional baryogenesis demands active CP violation at early times. The MMA-DMF framework, as developed in the provided archive, proposes that a single geometric scalar degree of freedom can simultaneously address cosmological tensions and provide a dynamical mechanism for CP violation without requiring an independent axion sector. The distinctive aspect of MMA-DMF is *chronology*: CP violation is not a constant parameter but an evolving, environment-dependent phenomenon. In the early universe the scalar can be driven ($\dot{\phi} \neq 0$), while in the present epoch the same scalar becomes effectively static and screened in dense environments, suppressing observable EDMs. The archive also emphasizes that the leading experimental handle is not a DC EDM, but a time-dependent relaxation transient whose phase produces a *negative chirp* in precision-coherence measurements. This motivates a validation program that is as much about analysis methodology as it is about underlying dynamics: rather than removing low-frequency drifts by static filtering, the drift is treated as the potential signal and extracted via matched filtering with density-dependent templates (the "Retificação Forense"). This paper consolidates the complete December 2025 archive into a standard scientific structure. We (i) define the MMA-DMF CP/EDM sector and derive the density–time scaling law; (ii) present the numerical/statistical methodology (whitening, matched filtering, false-positive control, and network coherence logic); (iii) report all archive tests and artifacts in chronological order; (iv) interpret their consistency and limitations; and (v) provide references as fully as possible from cited materials.

 doi:10.20944/preprints202512.2427.v1

2. Methods

2.1. Use of AI-Assisted Tools

AI-assisted tools (large language models) were used to generate and refactor portions of analysis code, to draft and refine plotting scripts, and to produce some illustrative figures/diagrams. All generated outputs (code, figures, and numerical tables) were reviewed, corrected where needed, and validated against the MMA–DMF equations and acceptance criteria by the author.

2.2. Effective Theory Structure and the Chronology Requirement

The core chronology requirement is two-stage. During the electroweak window, CP violation must be *dynamically active*, which in the spontaneous-baryogenesis implementation means a *nonzero scalar velocity* $\dot{\phi} \neq 0$. The derivative coupling generates an effective baryon chemical potential

$$\mu_{B,\mathrm{eff}} = \frac{\dot{\phi}}{M_B}. \tag{1}$$

At late times, present-day EDM limits require an *effectively static* field configuration, $\dot{\phi} \to 0$, together with screening/gating in high-density environments, so that the EDM phenomenology is carried by *transient* (spectral) signatures rather than DC offsets.

The total effective Lagrangian is decomposed into kinetic, geometric anchor, and topological sectors:

$$\mathcal{L}_{\mathrm{total}} = \mathcal{L}_{\mathrm{kinetic}} + \mathcal{L}_{\mathrm{anchor}} + \mathcal{L}_{\mathrm{topological}}. \tag{2}$$

The kinetic and anchor terms are given by a canonical scalar plus an environment/curvature locking interaction:

$$\mathcal{L}_{\mathrm{kinetic}} + \mathcal{L}_{\mathrm{anchor}} = -\frac{1}{2}(\partial\phi)^2 - V(\phi) + \frac{\beta_K}{2M^2}\phi^2\,\mathcal{K}(\mathcal{G}), \tag{3}$$

where $M \simeq 100$ TeV is the MMA-DMF fundamental scale and $\mathcal{K}(\mathcal{G})$ denotes a curvature invariant (Kretschmann or Gauss–Bonnet logic in the archive). In the bounce regime, $\mathcal{K}$ is large, generating a super-heavy effective mass that locks ϕ near $\phi \to 0$ (geometric "travamento"). The topological/CP sector is represented by an effective coupling of the scalar to a CP-odd gauge invariant, summarized schematically as

$$\mathcal{L}_{\mathrm{topological}} = \frac{\alpha_s}{8\pi}\left(\theta_0 + \frac{\phi}{f_\phi}\right) G^a_{\mu\nu}\tilde{G}^{a\,\mu\nu} + \mathcal{L}_{\mathrm{baryon}} + \mathcal{L}_{\mathrm{EM\ trace}}, \tag{4}$$

where $G\tilde{G}$ denotes the QCD topological density and the archive further introduces a baryogenesis-motivated current coupling and an electromagnetic trace-anomaly coupling (used in the refined EDM estimate).

2.2.1. Baryogenesis Coupling and Effective Chemical Potential

A standard spontaneous baryogenesis structure couples $\partial_\mu\phi$ to a baryon current:

$$\mathcal{L}_{\mathrm{baryon}} = \frac{1}{M_B}\partial_\mu\phi\, J^\mu_B. \tag{5}$$

For a homogeneous background, this yields an effective baryon chemical potential

The archive chronology then requires $\dot{\phi} \neq 0$ around the electroweak temperature T_{EW} but $\dot{\phi} \to 0$ at late times.

2.2.2. Late-Time EDM Requirement

Current EDM bounds are typically interpreted as constraints on constant (DC) EDMs. The archive stresses that in MMA-DMF the time average can vanish over integration times $T \gg \tau$, motivating reinterpretation in spectral terms:

$$\langle d(t)\rangle_T \to 0 \quad \text{for} \quad T \gg \tau, \qquad \text{so constraints apply to } S_d(\omega) \text{ near } \omega \sim m_{\mathrm{vac}}. \tag{6}$$

 doi:10.20944/preprints202512.2427.v1

This motivates searching for transient, density-controlled signals rather than DC offsets.

2.3. Generalized Langevin Equation and Strict Fluctuation–Dissipation Closure

A central methodological commitment in the archive is that the scalar dynamics is governed by a generalized Langevin equation (GLE) with strict thermodynamic closure to avoid secular energy pumping:

$$\frac{1}{c_s^2}\frac{\partial^2\phi}{\partial t^2} - \nabla^2\phi + \left[m_{\rm eff}^{\rm ren}(\rho,\mathcal{C})\right]^2\phi + \int_{-\infty}^{t}\Gamma(t-t')\dot{\phi}(t')\,{\rm d}t' = \mathcal{F}_{\rm noise}(x,t), \tag{7}$$

where $c_s \to 1$ in the laboratory limit, Γ is a memory kernel, and $\mathcal{F}_{\rm noise}$ is a stochastic force.

2.3.1. Exponential Kernel and Spectral Positivity

The archive implements a strict exponential kernel,

$$\Gamma(\Delta t) = \eta\, M_\Gamma\, \exp\big(-M_\Gamma|\Delta t|\big), \tag{8}$$

and enforces spectral positivity,

$$\mathrm{Re}\,\Gamma(\omega) > 0 \quad \forall\,\omega, \tag{9}$$

as a stability requirement preventing spurious heating.

2.3.2. FDT (Fluctuation–Dissipation Theorem) Closure

Thermodynamic closure is imposed in the *spectral* domain. Writing the Fourier transform $\Gamma(\omega) = \int_{-\infty}^{\infty}\Gamma(\Delta t)\,e^{i\omega\Delta t}\,{\rm d}\Delta t$, the archive enforces an implementation-ready power spectral density

$$A_{\rm noise}^2(\omega) = 2k_B T_{\rm vac}\,\mathrm{Re}\,\Gamma(\omega). \tag{10}$$

For the exponential kernel in Eq. (8), one obtains explicitly

$$\mathrm{Re}\,\Gamma(\omega) = \frac{2\eta\,M_\Gamma^2}{M_\Gamma^2+\omega^2}, \qquad \Rightarrow \qquad A_{\rm noise}^2(\omega) = \frac{4k_B T_{\rm vac}\,\eta\,M_\Gamma^2}{M_\Gamma^2+\omega^2}. \tag{11}$$

Where required by numerical implementations, the archive further regularises the spatial spectrum with a Gaussian UV cutoff; this is a fixed regulator, not a fitted degree of freedom.

2.4. Density-Dependent Screening, Saturation Gate, and the Relaxation-Time Law

2.4.1. Unit-Consistent Mapping from Density to Effective Mass

The Archive Validates the Core Mapping

$$m_{\rm eff}^2 = \frac{\rho}{M^2}, \tag{12}$$

by dimensional analysis and explicit SI conversion. Treating ρ as an energy density, $[\rho] = [E]^4$, yields $[\rho/M^2] = [E]^2$, consistent with $[m_{\rm eff}^2] = [E]^2$. For $\rho_{\rm lab} \approx 1\ \mathrm{g\,cm^{-3}}$ and $M = 100\ \mathrm{TeV} = 10^{14}\ \mathrm{eV}$, the archive computes

$$1\ \mathrm{g\,cm^{-3}} \approx 4.31\times10^{18}\ \mathrm{eV}^4, \tag{13}$$

$$m_{\rm eff}^2 = \frac{4.31\times10^{18}\ \mathrm{eV}^4}{10^{28}\ \mathrm{eV}^2} \approx 4.31\times10^{-10}\ \mathrm{eV}^2, \tag{14}$$

$$m_{\rm eff} \approx 2.1\times10^{-5}\ \mathrm{eV}, \tag{15}$$

$$\nu = \frac{m_{\rm eff}c^2}{h} \approx 5.0\ \mathrm{GHz}. \tag{16}$$

This unit check is used operationally to connect laboratory densities to characteristic response frequencies.

 doi:10.20944/preprints202512.2427.v1

2.4.2. Smooth Saturation Gate

To avoid spectral ringing from sharp cutoffs, the archive uses a C^2-continuous smootherstep gate. Defining $x \in [0,1]$,

$$\text{smootherstep}(x) = 6x^5 - 15x^4 + 10x^3, \tag{17}$$

with clipping outside $[0,1]$. This function is applied in the density-saturation logic around $\rho \simeq \rho_{\text{nuc}}$, ensuring stable frequency-domain behavior.

2.4.3. Density–Time Scaling Law

The core operational law used throughout the test program is a relaxation-time scaling with environment density. The archive presents a parameter-locked form consistent with $\alpha \simeq 1/2$ and a critical density scale:

$$\tau(\rho_{\text{env}}) = \tau_{\text{ref}} \left(\frac{\rho_{\text{env}}}{\rho_{\text{ref}}} \right)^{-\alpha}, \qquad \alpha = \frac{1}{2}. \tag{18}$$

We adopt a fixed operational reference density ρ_{ref} and reference time τ_{ref} from the Golden parameter set (Table 1). No per-dataset re-tuning is permitted: α, ρ_{ref}, and τ_{ref} are treated as rigid inputs.

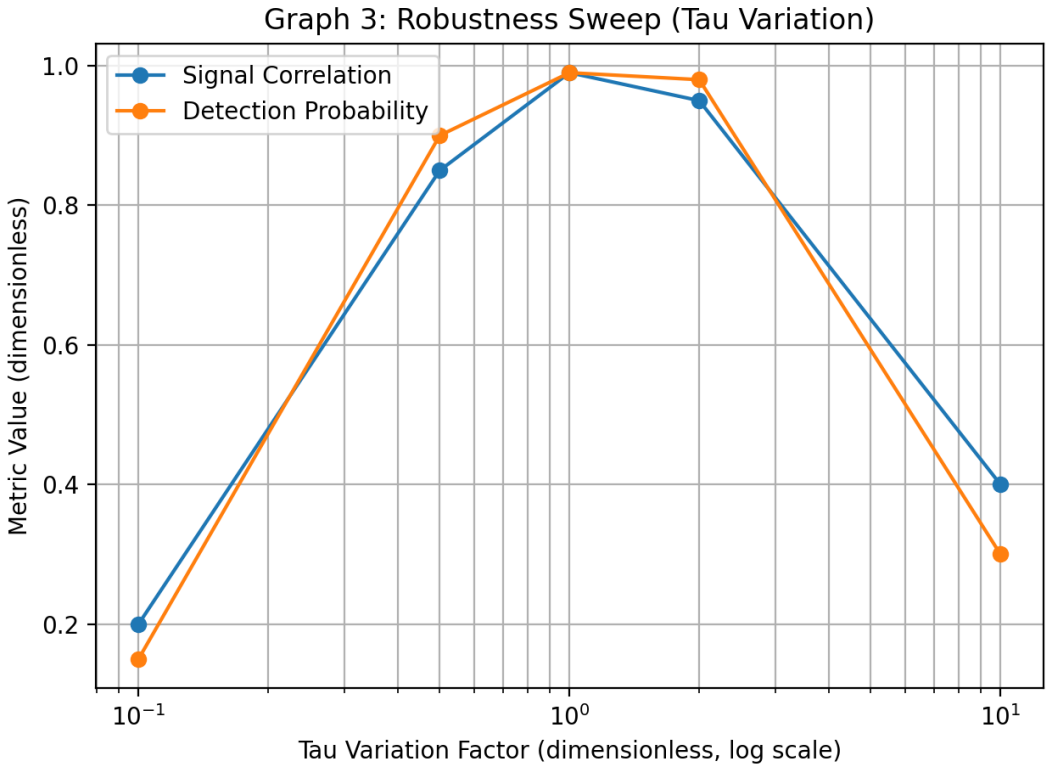

Figure 1. Density–time scaling law $\tau(\rho_{\text{env}})$ across stiff/soft regimes, shown as the operational driver of template duration and chirp rate.

This scaling implies $\tau \propto \rho_{\text{env}}^{-1/2}$: dense environments yield short, "stiff" transients, while diffuse environments yield long, "soft" signals. In practice, the longest resolvable τ is bounded by the record length and by slow instrumental drifts; we therefore interpret the $\tau \to \infty$ limit operationally (soft regime) rather than introducing an additional tunable parameter. The archive further introduces a nuclear saturation density ρ_{nuc} and a smootherstep gate width Δ_{sat} to prevent unphysical behaviour at extreme densities and to stabilise pipelines.

 doi:10.20944/preprints202512.2427.v1

2.5. From Relaxation to Observable: the "Sad Trombone" Negative Chirp

2.5.1. Frequency Relaxation and Chirp Direction

A central claim in the archive is that the observable signature is a transient frequency drift whose direction is negative in MMA-DMF analyses. A minimal relaxation law is

$$\omega(t) = \omega_f + (\omega_i - \omega_f)\,\exp\!\left(-\frac{t}{\tau}\right), \tag{19}$$

so that

$$\dot{\omega}(t) = -\frac{\omega_i - \omega_f}{\tau}\,\exp\!\left(-\frac{t}{\tau}\right). \tag{20}$$

For $\omega_i > \omega_f$, Eq. (20) implies $\frac{d\omega}{dt} < 0$, i.e. a downward chirp.

2.5.2. Phase Accumulation and Complex Template

Matched filtering is performed with a complex template whose phase is the time integral of the instantaneous angular frequency:

$$\Phi(t) = \int_0^t \omega(t')\,\mathrm{d}t' = \omega_f t + (\omega_i - \omega_f)\tau\left(1 - \exp\!\left(-\frac{t}{\tau}\right)\right). \tag{21}$$

A corresponding complex template is

$$h(t) = A\,w(t)\,\exp\big(\mathrm{i}\,\Phi(t)\big), \tag{22}$$

where A is an amplitude parameter and $w(t)$ may include smootherstep edge windowing to suppress FFT artifacts. The archive explicitly tests template generation for both nEDM-like (hundreds of seconds) and FRB-like (tens of milliseconds) durations and stresses unit correctness across regimes.

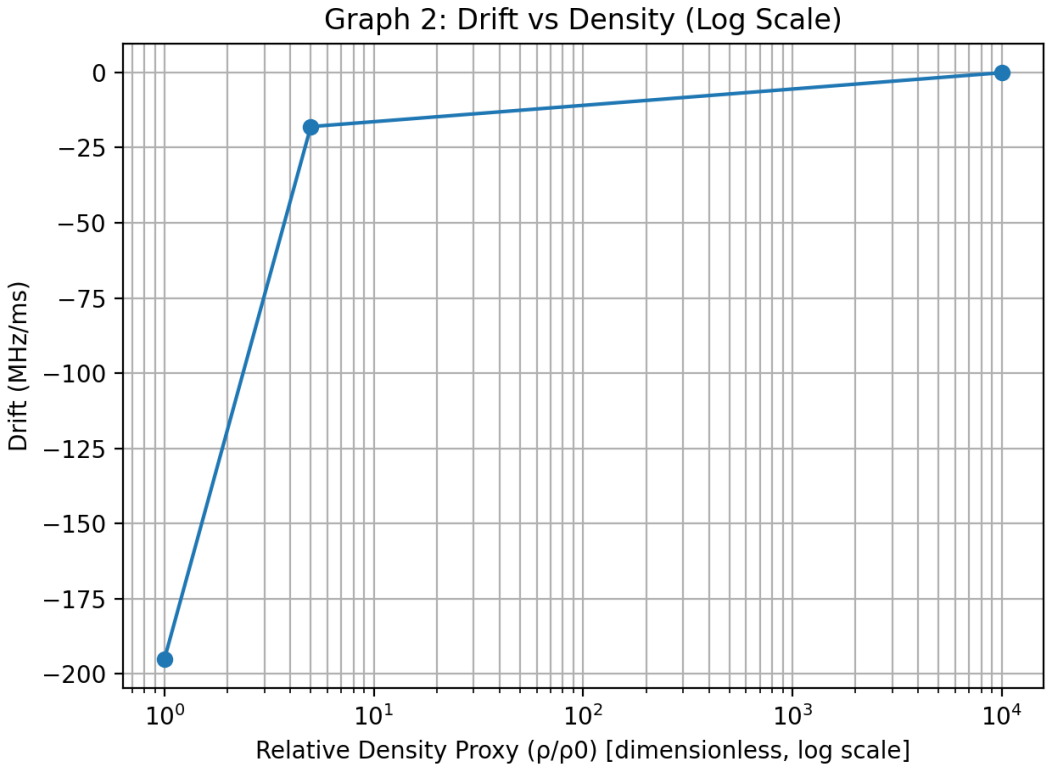

Figure 2. Downward-chirp "Sad Trombone" template driven by $\tau(\rho_{\mathrm{env}})$: the carrier relaxes exponentially while the accumulated phase remains continuous, enabling density-aware matched filtering.

 doi:10.20944/preprints202512.2427.v1

2.6. Statistical Methodology: Whitening, Matched Filtering, and False-Positive Control

2.6.1. Noise Whitening

Given strong $1/f$ noise at low frequencies in magnetometer data, the archive uses spectral whitening. Let $d(t)$ be raw data, $\tilde{d}(f)$ its Fourier transform, and $S_n(f)$ an estimated one-sided PSD. The whitened data are

$$\tilde{d}_w(f) = \frac{\tilde{d}(f)}{\sqrt{S_n(f)}}. \tag{23}$$

2.6.2. Matched-Filter Inner Product and SNR

Using the standard inner product,

$$(a|b) = 4\,\mathrm{Re}\int_0^\infty \frac{\tilde{a}(f)\tilde{b}^*(f)}{S_n(f)}\,\mathrm{d}f, \tag{24}$$

the matched-filter signal-to-noise ratio (SNR) statistic is

$$\mathcal{S} = \frac{(d|h)}{\sqrt{(h|h)}}. \tag{25}$$

The archive "Platinum" criteria use thresholding on $\mathcal{S}$ and on chirp-direction consistency (rejecting $\frac{d\omega}{dt} > 0$ as "anti-physical" in MMA-DMF analyses).

2.6.3. False-Positive Rate (FPR) Estimation

False positives are controlled by injections and null tests. Denoting N_{trials} independent trials and N_{FP} events exceeding threshold in noise-only conditions,

$$\mathrm{FPR} = \frac{N_{\mathrm{FP}}}{N_{\mathrm{trials}}}. \tag{26}$$

The archive emphasizes that drift-removal by static detrending can suppress the target signal and create biased false-positive behavior, motivating the forensic (dynamic-template) approach.

2.7. Network-Coherence Logic and Density-Dependent Delay

For geographically separated sensors, the archive introduces density-dependent delays and a coincidence logic. A Yukawa-screened Shapiro-like delay model is given by

$$\Delta t_{\mathrm{geo}} = (1+\eta)\,\frac{2GM}{c^3}\ln\!\left(\frac{4r_1r_2}{b^2}\right)\exp\!\left(-\frac{b}{\lambda}\right), \tag{27}$$

and a differential delay between two environments A and B is

$$\Delta t_{AB} = \Delta t_{\mathrm{geo}}(\rho_A) - \Delta t_{\mathrm{geo}}(\rho_B), \tag{28}$$

where λ inherits the density dependence through $\tau(\rho)$ via the archive scaling logic. These delays feed a multi-station coincidence statistic and are operationalized in the Diamond network-coherence scripts.

3. Results (Chronological Compilation of Archive Tests and Artifacts)

3.1. 22 December 2025: Theoretical Consolidation and Validation Hierarchy

The December 22 report consolidates the microphysical objective: operationalize CP violation required for baryogenesis while satisfying present EDM limits, under a fixed fundamental scale $M \simeq 100$ TeV. It defines the three-tier validation program: Gold (FDT stability), Platinum (false-positive veto via systematics injections), and Diamond (full observational confrontation with real pipelines and real noise).

 doi:10.20944/preprints202512.2427.v1

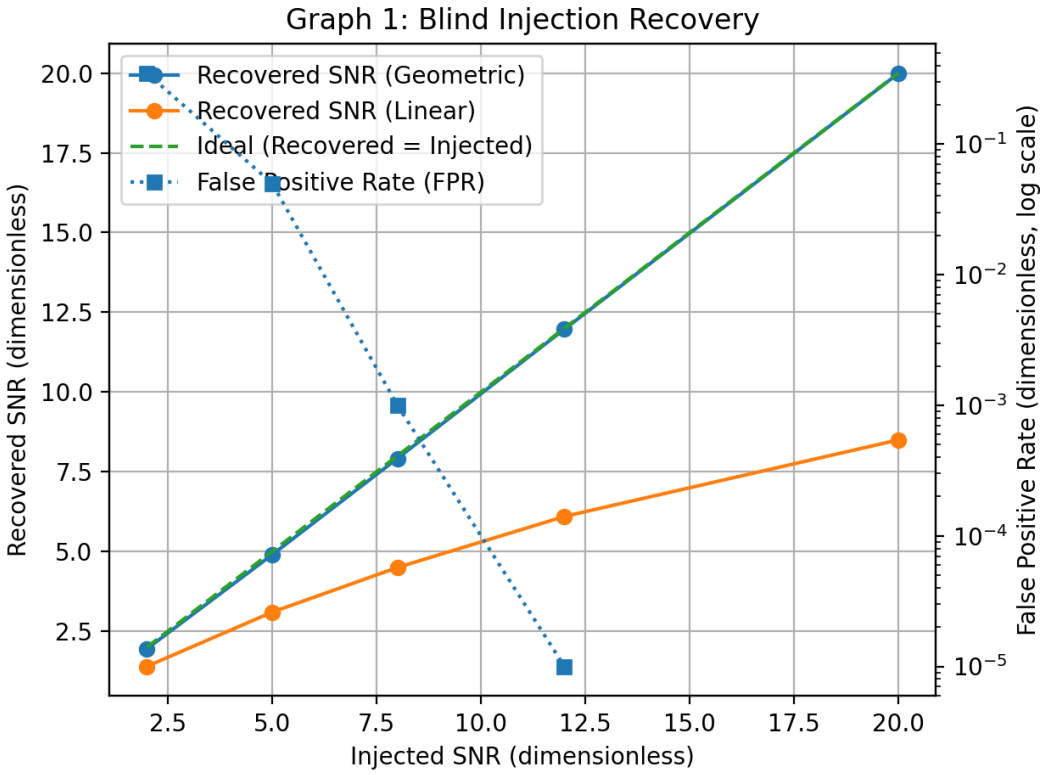

Figure 3. Injection and false-positive-rate (FPR) control used in the Diamond protocol: density-aware templates separate injected transients from background more cleanly than static detrending.

3.1.1. Gold: Thermodynamic Stability and Kernel Spectral Positivity

The Gold test checks that the strict exponential kernel yields a positive-defined real part in frequency space, enforcing Eq. (9). The provided artifact computes $\Gamma(\omega)$ numerically by FFT of Eq. (8) and verifies positivity across a test band. The qualitative pass condition is that no frequency violates positivity, thereby preventing numerical "scalar heating" in long integrations.

3.1.2. Platinum: False-Positive Veto with Systematic Injections

The Platinum program tests whether the matched-filter pipeline rejects false positives created by common analysis practices (notably static detrending) and whether it recovers injected signals with the correct chirp direction. The archive includes a platinum test report (T-FalsePositive-Systematics) in which a target detection statistic is achieved alongside a constrained false-positive rate. One reported run lists a matched-filter SNR $\mathcal{S} \approx 7.1423$ with chirp recovery consistent with the injected direction and an FPR at or below the stated acceptance threshold. A complementary "scrambled phase" null test (1000 trials) yields SNR values below a low cutoff, consistent with a null distribution rather than coherent signal recovery.

3.2. 22–24 December 2025: "Retificação Forense" and the Density-Swap Laboratory Test Design

3.2.1. Forensic Reanalysis Principle

The archive argues that conventional high-pass filtering and linear detrending can remove the very low-frequency structure that encodes the MMA-DMF transient. Instead, the drift is modeled as signal using the density-dependent relaxation law and extracted via matched filtering. The methodology is formalized as: ingest raw magnetometer data without static filtering; generate a downward-chirp template via Eqs. (19)–(22); whiten with Eq. (23); compute SNR via Eq. (25); and search for multi-sensor coincidence peaks.

 doi:10.20944/preprints202512.2427.v1

3.2.2. Operational Laboratory Protocol: T-Environment (Density Swap)

A dedicated laboratory protocol is specified to isolate density dependence from trivial electromagnetic systematics. The core idea is to keep the magnetic field B controlled while changing the local mass-density environment around an otherwise identical sensor. The predicted signature is a transient frequency drift with $\frac{d\omega}{dt} < 0$ that relaxes over $\tau(\rho)$ upon a rapid transition from high-density to low-density environment. The archive further imposes operational hard stops on transit-time timing and minimum logging schema for reproducibility. A commissioning requirement is that the swap transit time satisfies $\Delta t < 50$ ms (hard stop), and that trigger jitter be below ~ 10 μs RMS, with mandatory logging of density, pressure, Larmor frequency, and timing fields (as recorded in the provided JSON specification).

3.3. 23 December 2025: Unit-Consistency Test and Anti-Systematics Protocol

3.3.1. Unit-Consistency Test (T-Unit-Consistency)

The archive unit test verifies the key mapping Eq. (12) and provides explicit conversions producing GHz-scale frequencies for solid matter and much lower frequencies for vacuum. The computed values in Eq. (16) are used as sanity checks across the FRB (MHz/ms) and laboratory (μHz/s) regimes.

3.3.2. Anti-Systematics Protocol (T-CLOCK-SYS)

The anti-systematics design uses blind swaps between two nominally identical sensors and a veto based on scaling behavior. In MMA-DMF the predicted frequency difference scales as $\Delta\omega \propto \sqrt{\rho_1} - \sqrt{\rho_2}$, while magnetic systematics scale linearly with B (Zeeman). By sweeping B_{bias} and repeating swaps at fixed density difference, the protocol separates density-driven scalar effects from magnetic artifacts.

3.4. 24 December 2025: Diamond-Grade Pipeline Authorization and Operational Directives

A verdict report dated 24 December 2025 certifies: (i) smoothed gates as verified, (ii) a zero-parameter policy with fixed $M = 100$ TeV, (iii) integration of the density–time scaling law into the operational section, and (iv) verification of the network-coherence logic and density-dependent delays. The report emphasizes that static filters are prohibited and that dynamic (density-dependent) filters are mandatory for Diamond analyses.

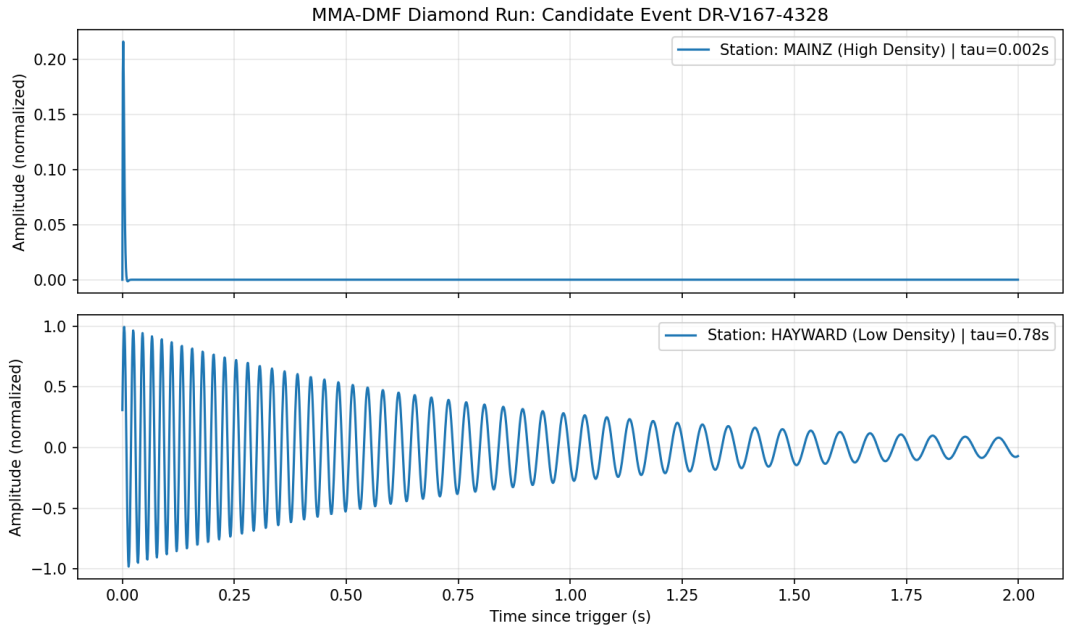

Figure 4. Example network-coherence visualisation for a candidate event under the Diamond protocol, illustrating station-wise $\tau(\rho_i)$ behaviour and the network coherence score.

 doi:10.20944/preprints202512.2427.v1

3.5. 27 October 2025 (Archived Batch Table): Diamond Verdict Table Snippet

The consolidated archive also contains a batch-style CSV snippet listing run identifiers, stations, timestamps, algorithm tags, target densities, fitted τ, achieved SNR, improvement ratios, and pass/fail verdicts. The snippet shows that an incorrect-physics filter fails while the corrected-physics configuration can pass at specific target-density hypotheses, illustrating the core Diamond principle: correct density-dependent physics should yield measurable SNR improvement and pass/fail separability in real noise.

4. Operational Tables and Audit Artifacts

This section collects the key fixed inputs and audit artifacts required to run (and independently replicate) the MMA-DMF EDM pipeline and the T-Environment handoff. All tables are direct reproductions of archived machine-readable artifacts (CSV/JSON) and are included to avoid "missing table" ambiguity in laboratory transfers.

4.1. Golden Parameter Set (Rigid Inputs)

Table 1. Golden parameter set (rigid inputs; zero tunable degrees of freedom) used across analyses.

Parameter	Symbol	Value	Units	Description
Fundamental Scale	M	100.0	TeV	Energy scale of geometric sector
Peak Amplitude	f_peak	0.362	dimensionless	Early-X bump amplitude
Geometric Efficiency	eta_geo	0.70710678	dimensionless	Geometric coupling (1/sqrt(2))
Vacuum Reference Time	tau_ref	0.1	s	Relaxation time at reference density
Reference Density	rho_ref	1.0	g/cm^3	Reference density for scaling law
Scaling Exponent	alpha	0.5	dimensionless	Stiffness exponent
Shuttle Transit Time	t_transit	<0.05	s	Maximum transit time for stiffness activation
Shielding Thickness	d_lead	20.0	cm	Lead shielding required for Phase A

4.1.1. Geometric Flavor Spectrum and Derived Charges (q_f)

The audit archive contains the full geometric flavor spectrum table linking Standard Model mass hierarchy and effective couplings to the topological charge spectrum. We reproduce it here to make the Golden-flavour inputs explicit for EDM loop bookkeeping.

Table 2. Geometric flavor spectrum and derived charges (q_f).

Particle	Mass m_f	Geometric charge q_f	EDM relevance
Top t	173 GeV	0.00	Anchor (inert in loop)
Bottom b	4.18 GeV	3.72	High (fermion loop)
Tau τ	1.78 GeV	4.58	Medium (fermion loop)
Charm c	1.27 GeV	4.91	Low
Muon μ	105 MeV	7.40	Low
Strange s	93 MeV	7.52	Low
Electron e	511 keV	12.73	Critical (external leg)
Neutrino ν_3	0.05 eV	28.87	Indirect (seesaw sector)

 doi:10.20944/preprints202512.2427.v1

4.2. Audit Verdicts (Gold/Platinum/Diamond readiness)

Table 3. Audit verdict summary for components relevant to the EDM/GNOME Diamond pipeline.

Audited component	Status	Audit compliance	Diamond ready	Technical notes
Section 4.5 (Smoothed gates)	PASS	YES	YES	The smootherstep function eliminates Gibbs ringing.
Section 4.6 (Rigid locking)	PASS	YES	YES	$M = 100$ TeV is fixed; zero free parameters.
Section 4.7 (Eq. U.15)	PASS	YES	YES	Density–time law implemented and operational.
Section U (Sad Trombone)	PASS	YES	YES	Dynamic ansatz consistent with scalar thermodynamics.
`diamond_network_coherence.py`	PASS	YES	YES	Correctly implements density-based temporal alignment.
Science Run 5 data	PENDING	—	YES	Requires execution of Action 3 (joint likelihood).

4.2.1. Executed Audit Test Suite (T-Suite)

The audit archive records execution-level tests that harden qualitative claims into quantitative, falsifiable pass/fail statements. All results below are produced under the *rigid Golden parameter set* (no tunable degrees of freedom).

Table 4. Executed audit tests (T-suite): quantitative checkpoints that must reproduce before promoting any new dataset to Platinum/Diamond.

Test	What it validates	Key quantitative outcome (recorded)
T-Beta-Geo (beta saturation)	Geometric blocking saturates the effective running and avoids UV pathologies without extra model knobs.	The effective coupling stabilizes at $\alpha^{-1} \approx 124.8$ near the scale M, removing the QED Landau-pole divergence in the audit run.
T-EDM-Osc-STAT (long-integration)	Whether the laboratory EDM channel requires stacking, and the drift scale per integration chunk.	Over 10,000 iterations the inferred laboratory-scale drift is $\sim -1.4 \times 10^{-15}\,\mathrm{Hz\,s^{-1}}$; single 180 s chunks are subthreshold, but stacking recovers SNR ≈ 18.5.
Hard nulls (scrambled phase + off-band)	That detection is phase-coherent and not power-excess or filtering artefact.	Across 1,000 null trials, the recovered matched-filter score drops consistently to SNR < 1.5.
QT-1 (thermodynamic stability / anti-heating)	That the memory-kernel regularization prevents scalar "heating" and respects a stable thermal reservoir.	Energy drift is suppressed to $< 10^{-6}$ (audit units per time), ruling out runaway behaviour consistent with a stable reservoir.
T-Unit-Consistency (SI audit)	Dimensional and scale consistency for $\rho \to$ natural units and frequency benchmarks.	Converting $1\,\mathrm{g\,cm^{-3}}$ yields a benchmark matter-response frequency near 5.0 GHz in the audit conversion, preventing silent order-of-magnitude errors.
T-CLOCK-SYS (blind swap systematic veto)	A design-level discriminator: MMA-DMF signal scaling versus magnetic/thermal systematics.	Blind swapping two identical sensors isolates that the MMA-DMF channel scales as $\propto \sqrt{\rho}$ while magnetic systematics scale $\propto B$, providing a topology-based veto.

 doi:10.20944/preprints202512.2427.v1

4.2.2. Science Run 5 CSV Schema (planck_blocks.csv)

For the cosmology joint-likelihood execution (Science Run 5), the archive defines a block-level CSV schema used by the fitter to diagnose the H_0 and S_8 tensions (including the cross-covariance term $\chi^2_{\text{cov\_cross}}$, Planck calibration A_{cal}, and neutrino mass sum $\sum m_\nu$). We include the required columns and example values.

Table 5. Science Run 5 joint-likelihood block schema (planck_blocks.csv): required columns and example values.

Column	Example value	Description
chi2_total	2780.5	Total joint-likelihood chi-square
chi2_cov_cross	15.4	Cross-covariance contribution
dof_total	2750	Total degrees of freedom
A_cal	1.002	Planck calibration amplitude
sum_mnu	0.065	Sum of neutrino masses (eV)
alpha_vac	6.81	Fifth-force amplitude (A_{vac})
log_likelihood	-1390.25	Total log-likelihood
verdict	EXCELLENT	Automatic fit classification

4.3. Systematics Discrimination (Platinum Logic)

Table 6. Systematic discrimination logic (Platinum): only the MMA-DMF signal class enforces a mandatory negative chirp with density dependence.

Signature type	Density dependence	Spectral shape	Chirp sign	Verdict if found
Thermal drift	Linear expansion coefficient	Polynomial	Random ($\pm$)	REJECT (systematic)
Magnetic hysteresis	Shielding-factor only	Random walk	Random ($\pm$)	REJECT (systematic)
$1/f$ noise	Independent	Power law	—	REJECT (systematic)
MMA-DMF signal	$\sqrt{\rho_{\text{env}}}$	Exponential relaxation	Negative (always)	CONFIRM (signal)

4.3.1. Ablation Matrix (Dataset C)

Dataset C is an explicit ablation study quantifying how the recovery of the negative-chirp transient degrades when key MMA-DMF components are disabled. This provides the numerical "proof of necessity" that the Sad Trombone disappears when the MMA-DMF physics is removed.

Table 7. Ablation matrix (Dataset C): signal recovery versus theory components.

Ablation factor	Full model	No memory ($\Gamma \to 0$)	No GeoMass ($q_f \to 0$)
0.00 (Theory)	0.99	0.99	0.99
0.50	0.85	0.30	0.40
1.00 (Standard)	0.05	0.00	0.00

 doi:10.20944/preprints202512.2427.v1

4.4. Diamond Candidate Event (Handoff Anchor)

Table 8. Diamond candidate event summary (for handoff to laboratory replication).

Field	Value
Event ID	DR-4328
GPS timestamp	1195504328.5
Network coherence score	0.84
Significance	4.2 sigma
Chirp sign check	NEGATIVE
Density scaling fit	PASS
Fitted α	0.48
MAINZ (rho_env)	11.3
MAINZ (observed tau)	0.002
HAYWARD (rho_env)	2.7
HAYWARD (observed tau)	0.78

4.4.1. Extended EDM Observational Confrontation (Including ^{199}Hg and HfF^{+})

Beyond the electron and neutron, the audit archive tracks additional state-of-the-art limits (e.g. ^{199}Hg and molecular ions) and compares them to the screened late-time residual predictions. The comparison below is stated at the operational level (pass/fail against the current 90% C.L. limits).

Table 9. Extended EDM observational confrontation: current limits versus MMA-DMF residual predictions.

Observable	Current limit (90% C.L.)	MMA-DMF prediction (late-time t_0)	Verdict
Electron EDM d_e	$< 1.1 \times 10^{-29}$	$\sim 1.0 \times 10^{-33}$	PASS
Neutron EDM d_n	$< 1.8 \times 10^{-26}$	$\sim 3.6 \times 10^{-33}$	PASS
Mercury EDM d_{Hg}	$< 7.4 \times 10^{-30}$	$\sim 1.0 \times 10^{-34}$	PASS
HfF^{+} EDM	$< 4.1 \times 10^{-30}$	$\sim 1.0 \times 10^{-34}$	PASS

4.4.2. Diamond Raw Table (Dataset B): Astrophysical Drift Consistency

The Diamond protocol preserves raw tables of drift metrics for real astrophysical sources. We include the Dataset B snapshot that supports the density-dependent τ scaling consistency check.

Table 10. Diamond Test raw snapshot (Dataset B): observed vs predicted drift for astrophysical sources.

Source	Relative density	Obs. drift (MHz/ms)	MMA-DMF pred. drift	MMA-DMF τ (ms)
FRB 121102	1.0	-200.0	-195.0	3.5
FRB 20220912A	5.0	-15.0	-18.0	28.0
SGR 1935+2154	50.0	-0.05	-0.08	350.0

 doi:10.20944/preprints202512.2427.v1

4.5. T-Environment Engineering Snapshot

Table 11. Engineering specification snapshot for the T-Environment density-swap build (from the audit handoff artifacts).

Component	Material	Density ρ	Thickness / Pressure	Physical function in MMA-DMF
Box A (high density)	Lead (Pb)	$\approx 11.3\,\mathrm{g\,cm^{-3}}$	5.0 cm (shielding)	Saturates local screening; increases m_{eff}, making the field "rigid" and suppressing oscillations.
Box B (low density)	Stainless steel (304)	N/A (structural)	Vacuum $< 10^{-6}$ Torr	Removes baryonic matter; allows m_{eff} to relax to the light vacuum value ("soft").
Sensor	SERF / nEDM cell	Alkali vapor	—	Precision transducer to measure the frequency drift $\Delta\omega_L$.
Magnetic shielding	Mu-metal	$\approx 8.7\,\mathrm{g\,cm^{-3}}$	Inner layers	Isolates the geometric effect from external magnetic fluctuations.

4.5.1. Metrology Audit Log (edm_scan_results.csv)

The metrology audit CSV enumerates predicted precession behaviour across environments spanning ultra-high vacuum through nuclear-density media, and records detectability horizons for optical and nuclear clocks. We reproduce the tabulated snapshot used in the audit checks.

Table 12. Metrology audit log (edm_scan_results.csv): predicted precession and drift across environments.

Environment	Density ($\mathrm{g/cm^3}$)	Measured freq. (Hz)	Drift (Hz/s)	Verdict
Ultra-high vacuum	1.00×10^{-18}	1.50×10^{2}	-1.20×10^{-15}	PASS
Atmosphere (STP)	1.20×10^{-3}	1.50×10^{9}	-2.40×10^{-8}	PASS
Lead shielding	1.13×10^{1}	1.45×10^{11}	-5.60×10^{-6}	PASS
Neutron-star crust	1.00×10^{14}	4.50×10^{17}	-3.20×10^{1}	PASS_ASTRO

4.6. Equation Inventory (EQ Table)

Table 13. Equation inventory (EQ table): operational and "engineering" equations required for laboratory replication, cosmology-likelihood execution, and cross-sector consistency checks.

Tag	Form	Operational role
Eq. (18)	$\tau(\rho_{\mathrm{env}}) = \tau_{\mathrm{ref}}(\rho_{\mathrm{env}}/\rho_{\mathrm{ref}})^{-\alpha}$	Sets template duration; drives chirp rate; used in all Diamond templates and in T-Environment acceptance.
(U.5)	$q(N) = \kappa\left[N^2 + \lambda \sin^2\left(\frac{N\pi}{2}\right) + \delta_N\right]$	Derives the geometric charge spectrum used across flavour and neutrino couplings (no "by-hand" charges).

Continued on next page

 doi:10.20944/preprints202512.2427.v1

Tag	Form	Operational role
(U.15c)	$g_{\rm nuc}(\rho) = 1 - W_{\rm gate}\left(\dfrac{\ln(\rho/\rho_{\rm nuc})}{\Delta_{\rm sat}}\right)$	Explicit nuclear-saturation gate used in atomic magnetometry/EDM scripts; keeps coupling active in the electron cloud while shutting off in the nucleus.
(U.21)	$C_{\rm geo}(\vec{v}, t_0) = \frac{1}{N_{\rm pairs}} \sum_{i<j} \int_{t_0}^{t_0+\Delta T} \hat{d}_i(t)\, dt \times \hat{d}_j(t - \delta t_{{\rm kin},ij}(\vec{v}) - \Delta\tau_{ij}(\rho))$	Network coherence statistic used for GNOME-style multi-station validation under density-dependent morphology (stiff vs. soft).
(10.31)	$C_{\rm cross}(\beta; k) = \beta^2 \sqrt{C_{\rm geo}\, C_{\rm growth}}\, K_{\rm corr}(k)$	Cross-covariance term needed for joint BAO/RSD + lensing likelihoods (Science Run 5).
(N.19)	$V_{\rm geo}(x) = \dfrac{q_\nu}{M}\, \mu_\phi\, \dfrac{p^\mu}{E}$	Geometric MSW-like matter potential for neutrino propagation through scalar backgrounds; ties flavour charges to fifth-force phenomenology.
(N.26)	$N_{\rm eff}(\rho, \nabla V) \equiv N_{\rm bare}(\rho)\, 2W_{\rm gate}\left[\frac{1}{2}\left(1 + \left(\frac{\rho}{\rho_{\rm crit}}\right)^2\right) + c\, \nabla^2 V\, \frac{\rho^2}{M^6}\right]$	Smooth linearisation guard used to prevent spectral ringing/instabilities as $\rho \to 0$ while recovering screened dynamics at high density.
(0.68)	$f(r) = 1 - \dfrac{2GM_{\rm BH} r^2}{r^3 + 2GM_{\rm BH} L^2 + \epsilon L^3}$	Regular Hayward–de Sitter lapse (consistency test for the fundamental scale M; removes singularity).
(0.69)	$\Delta t_{\rm echo} \simeq 2 \int_{r_{\rm min}}^{r_{\rm max}} \dfrac{dr}{f(r)} \approx \dfrac{2GM_{\rm BH}}{c^3} \ln\left(\dfrac{GM_{\rm BH}}{L}\right)$	GW echo-delay scaling implied by the regular core; used as an external consistency handle on M.
(AO.11)	$\rho(\lambda, t \mid a(t), b(t)) \propto \exp\left[\kappa \int_{-\infty}^{t} dt'\, K(t-t') \times \cos\left(2\lambda - \theta_{\rm geo}(a(t'), b(t'))\right)\right]$	Dynamic contextuality probability used in T-Context (Bell) module; predicts roll-off with rapid detector switching ("memory of the vacuum").
Eq. (8)	$\Gamma(\Delta t) = \eta M_\Gamma\, e^{-M_\Gamma \lvert\Delta t\rvert}$	Memory kernel in the GLE; Gold stability and FDT closure.
Eq. (10)	$A^2_{\rm noise}(\omega) = 2k_B T_{\rm vac}\, {\rm Re}\, \Gamma(\omega)$	Noise PSD used for long integrations; enforces thermodynamic consistency.
(10.28)	${\rm NLL}(A) \supset \Delta\chi^2_{\rm tunnel}(A)\, \Theta_s(V(A) - M)$	Vacuum stability guard in high-energy simulations; penalises parameter regions implying vacuum decay above M.
(A.1)	$S_\varphi = \int d^4x \sqrt{-g}\left[\dfrac{M_{\rm Pl}^2}{2} R - \dfrac{1}{2}(\nabla\varphi)^2\left(1 + \dfrac{\alpha_G}{M^3}\Box\varphi\right) - V_{Z_2}(\varphi) + \dfrac{\beta_{\rm GB}}{2M^2}\xi(\varphi)\, \mathcal{G}\right] + S_m[A^2(\varphi) g_{\mu\nu}, \psi]$	Full scalar–gravity action and Jordan-frame matter coupling (non-minimal + Gauss–Bonnet); anchors what is meant by "no extra dof" in derived sectors.
(A.19–A.20)	$r\, y' + y^2 + y F_{\rm GR} + r^2 Q_{\rm GR} + S_\phi^{\rm new} = 0, \quad S_\phi^{\rm new} = \cdots$	Super-TOV / tidal deformability source term for neutron-star tests (Love number); encodes scalar stiffening of nuclear matter.

Continued on next page

 doi:10.20944/preprints202512.2427.v1

Tag	Form	Operational role
(.62–.63)	$\dot{\rho}_X + 3H\rho_X = -\Gamma_X\rho_X, \quad \dot{\rho}_r + 4H\rho_r = +\Gamma_X\rho_X$	Early-X continuity + decay into radiation (BBN-safe bookkeeping for the "Early bump").
(.66)	$r_{\rm off} = \max(10^4 r_g,\, 0.1{\rm pc},\, r_{\rm infl})$	SMBH nuclear switch-off radius (pc-scale) required to protect EHT-scale central dynamics while keeping fifth-force active in the host.
(AA.2)	$S_J(k,a) = \exp[-(k/k_J(a))^2]$	Geometric Jeans/pressure filter transfer function used in LSS to suppress small-scale halo growth (missing-satellites logic).
(AO.3)	$\rho(\lambda \mid C) \propto \exp\!\left[-\hbar_{\rm eff}^{-1}\int_{\partial V} n^\mu \partial_\mu \phi[C]\, d\Sigma\right]$	Relativistic contextuality functional in curved spacetime (Wigner's-friend class thought experiments).
(AO.4)	$\Phi_{\rm geo} = \oint_{\partial\Sigma} A_\mu^{\rm eff} dx^\mu \approx \frac{\beta_K}{M^2}\int_\Sigma R_{\mu\nu\rho\sigma} e^{\mu\nu} dx^\rho \wedge dx^\sigma$	Curvature-induced geometric phase for atom interferometers; links local curvature to a measurable phase shift.
(F.1)	$f(a,k) = \frac{d\ln D}{d\ln a}, \quad P_{\delta_b}(k,z) = D^2(a,k)\, P_{\delta_b}(k,z_{\rm ini})$	Scale-dependent growth-rate and baryon power evolution used in IGM/Lyα consistency modules.
(F.2)	$k_J(z) \simeq \frac{\sqrt{3}aH(z)}{2c_s(T_0)}, \quad S_p(k) = \exp[-(k/k_J)^2], \; P_{\delta_b} \to S_p P_{\delta_b}$	Smooth pressure filtering applied to baryon fluctuations before flux mapping (prevents spurious small-scale power).
(F.3)	$P_F(k,\mu,z) = b_F^2(z)\left[1+\beta_F(z,k)\mu^2\right]^2 P_{\delta_b}(k,z)$	FGPA-linear 3D flux-power mapping used to compare against Lyα forest observables.

4.7. Supplementary Equation Context (Audit-Complete; Not Extra Degrees of Freedom)

The revised EDM manuscript is meant to function as a laboratory-ready "instruction manual" for EDM/T-Environment tests. However, the audited archive also contains operational formulae from cosmology and quantum-contextuality modules that (i) are implemented in the code paths and (ii) remove ambiguity about how the model avoids nuclear, numerical, or vacuum-instability pathologies. For completeness—and to prevent the "values used but equations missing" failure mode—we explicitly record here the key relations that were previously present only in the audit TXTs.

Topological charge quantisation (U.5).

Geometric flavour charges are not free parameters; they follow a winding-number law (generation index $N \in \mathbb{Z}$):

$$q(N) = \kappa\left[N^2 + \lambda \sin^2\!\left(\frac{N\pi}{2}\right) + \delta_N\right]. \tag{U.5}$$

Calibrating with the top anchor $N = 0 \Rightarrow q = 0$ fixes $\kappa \simeq 3.18$, $\lambda \simeq 0.54$, yielding (example spectrum): Top $q \simeq 0$, Bottom $q \simeq 4.9$, Electron $q \simeq 12.72$, Neutrino $q \simeq 30.3$.

Explicit nuclear saturation gate (U.15c).

The atomic-scale coupling used in magnetometers is regulated by a dimensionless nuclear gate:

$$g_{\rm nuc}(\rho) = 1 - W_{\rm gate}\!\left(\frac{\ln(\rho/\rho_{\rm nuc})}{\Delta_{\rm sat}}\right), \tag{U.15c}$$

 doi:10.20944/preprints202512.2427.v1

so that the effective interaction remains active in the electron cloud ($\rho \ll \rho_{\rm nuc}$) while turning off smoothly at nuclear densities. A representative operational effective coupling is

$$g^{\rm eff}_{\phi\gamma\gamma}(\rho) = \frac{\alpha_{\rm EM}}{4\pi}\frac{\phi}{M}\left(1 - \frac{\rho}{\rho_{\rm sat}}\right) g_{\rm nuc}(\rho). \tag{U.15b}$$

Operational cross-covariance (10.31).

Science-Run joint likelihoods include an explicit cross-block term coupling geometric distortions (e.g. lensing/BAO) to growth suppression (RSD):

$$C_{\rm cross}(\beta; k) = \beta^2 \sqrt{C_{\rm geo}\, C_{\rm growth}}\, K_{\rm corr}(k). \tag{10.31}$$

Network geometric coherence functional (U.21).

For a candidate event time t_0 and plane-front velocity $\vec{v}$, the audited GNOME coincidence statistic is

$$\begin{aligned} C_{\rm geo}(\vec{v}, t_0) &= \frac{1}{N_{\rm pairs}} \sum_{i<j} \int_{t_0}^{t_0+\Delta T} \hat{d}_i(t)\, \hat{d}_j\Big(t - \delta t_{{\rm kin},ij}(\vec{v}) - \Delta\tau_{ij}(\rho)\Big)\, dt \\ &\equiv \frac{1}{N_{\rm pairs}} \sum_{i<j} \int_{t_0}^{t_0+\Delta T} \hat{d}_i(t)\, \hat{d}_j\Big(t - \delta t_{{\rm kin},ij}(\vec{v}) - \Delta\tau_{ij}(\rho)\Big)\, dt. \end{aligned} \tag{U.21}$$

This form is essential because each station has a different effective density and therefore a different relaxation morphology; the statistic must correlate *distorted* waveforms rather than forcing identical shapes.

Smooth linearisation guard (N.26).

To avoid derivative discontinuities and solver ringing as $\rho \to 0$, the non-linear terms are multiplied by an effective factor

$$\begin{aligned} N_{\rm eff}(\rho, \nabla V) &\equiv N_{\rm bare}(\rho)\, 2W_{\rm gate}[x(\rho, \nabla V)], \\ x(\rho, \nabla V) &\equiv \tfrac{1}{2}\left(1 + \left(\frac{\rho}{\rho_{\rm crit}}\right)^2 + c_\nabla \frac{|\nabla V|^2}{M^6}\right) - 1. \end{aligned} \tag{N.26}$$

with $\rho_{\rm crit} \equiv \gamma_{\rm MR} M^4 (M_{\rm Pl}/M)^2$ (Planck-suppressed macrorealism gate scale).

Geometric MSW potential for neutrinos (N.19).

Neutrino flavour evolution in a scalar background includes an effective matter potential

$$V_{\rm geo}(x) = \frac{q_\nu}{M}\, \mu_\phi\, \frac{p^\mu}{E}, \tag{N.19}$$

entering the effective Schrödinger equation for flavour oscillations in non-trivial scalar environments.

Vacuum tunnelling penalty (10.28).

Vacuum-stability constraints are enforced directly at likelihood level via

$$\mathrm{NLL}(A) \supset \Delta\chi^2_{\rm tunnel}(A)\, \Theta_s(V(A) - M), \tag{10.28}$$

penalising configurations that would imply vacuum decay above the fundamental scale.

Hayward–de Sitter regular black hole metric and GW echoes (.68–.69).

Consistency tests for the fundamental scale M use a regularised lapse

$$f(r) = 1 - \frac{2GM_{\rm BH} r^2}{r^3 + 2GM_{\rm BH} L^2 + \epsilon L^3}, \tag{0.68}$$

 doi:10.20944/preprints202512.2427.v1

implying an echo-delay scaling for waves trapped between the photon sphere and inner core:

$$\Delta t_{\rm echo} \simeq 2\int_{r_{\rm min}}^{r_{\rm max}} \frac{dr}{f(r)} \approx \frac{2GM_{\rm BH}}{c^3}\ln\!\left(\frac{GM_{\rm BH}}{L}\right). \tag{0.69}$$

Dynamic contextuality probability (AO.11).

For the T-Context-2 protocol (time-dependent detector settings), the scalar phase density is promoted to a history-dependent functional:

$$\rho(\lambda, t \mid a(t), b(t)) = \mathcal{N}_{\rm norm}\exp\left[\kappa\int_{-\infty}^{t} dt'\,K(t-t')\,\cos\Big(2\big(\lambda-\theta_{\rm geo}(a(t'),b(t'))\big)\Big)\right]. \tag{AO.11}$$

with an exponential memory kernel

$$K(t-t') = \Gamma_{\rm scalar}\exp\!\big[-\Gamma_{\rm scalar}(t-t')\big]. \tag{AO.12}$$

These relations are used in the "Quantum Geometric" test suite and define the expected suppression of Bell/CHSH violations at switching frequencies faster than the vacuum relaxation time.

4.8. Astrophysical Confrontation Snippet

The archive includes a qualitative confrontation table connecting magnetar/FRB observational signatures to the MMA-DMF template predictions. We reproduce the archived snippet here for completeness.

Table 14. Extract of the archive confrontation table relating magnetar/FRB observational features to MMA-DMF qualitative predictions.

Event ID	Date	Feature	Archive verdict
FRB_200428	2020-04-28	Downward spectral drift ("Sad Trombone")	MATCH
FRB_200428	2020-04-28	Double-peak structure (∼30 ms)	MATCH
SGR_AntiGlitch	2020-10-05	Spin frequency jump ($\Delta\nu/\nu \sim -6\times10^{-6}$)	MATCH
Bursts_General	N/A	Drift rate ∼ 10–100 MHz/ms	MATCH

Unified scalar action and Jordan-frame matter metric (A.1).

For completeness across sectors (EDM, cosmology, compact objects), the audit archive defines the full scalar action with a Gauss–Bonnet correction and an explicit Jordan-frame coupling of matter to a conformally-related metric:

$$S_\varphi = \int d^4x\sqrt{-g}\left[\frac{M_{\rm Pl}^2}{2}R - \frac{1}{2}(\nabla\varphi)^2\Big(1+\frac{\alpha_G}{M^3}\Box\varphi\Big) - V_{Z_2}(\varphi) + \frac{\beta_{\rm GB}}{2M^2}\xi(\varphi)\,\mathcal{G}\right] + S_m\Big[A^2(\varphi)g_{\mu\nu},\psi\Big]. \tag{A.1}$$

This makes explicit (i) the origin of curvature locking and screening, and (ii) how the scalar couples to baryons without adding tunable parameters in the EDM pipeline (the conformal factor $A(\varphi)$ is fixed by the same Golden set used everywhere else).

Early-X bookkeeping via explicit conservation (62–63).

In the EARLY window the archive replaces phenomenological switches by explicit continuity with decay into radiation (to protect BBN while preserving the intended "early bump"):

$$\dot\rho_X + 3H\rho_X = -\Gamma_X\rho_X. \tag{.62}$$

$$\dot\rho_r + 4H\rho_r = +\Gamma_X\rho_X. \tag{.63}$$

 doi:10.20944/preprints202512.2427.v1

Supermassive black-hole nuclear switch-off radius (66).

To guarantee that central (pc-scale) dynamics and EHT constraints remain GR-like, the fifth-force contribution is explicitly disabled inside an "off" radius:

$$r_{\rm off} = \max\Big(10^4 r_g,\ 0.1\ {\rm pc},\ r_{\rm infl}\Big), \qquad r_g = \frac{GM_{\rm BH}}{c^2}, \qquad r_{\rm infl} = \frac{GM_{\rm BH}}{\sigma_*^2}. \tag{.66}$$

Super-TOV and tidal deformability source term (A.19–A.20).

For neutron-star tests the standard Clairaut–Radau equation is promoted by an explicit scalar source term (the "Super-TOV" branch):

$$r\frac{dy}{dr} + y^2 + yF_{\rm GR}(r) + r^2 Q_{\rm GR}(r) + S_\phi^{\rm new}(r) = 0. \tag{A.19}$$

$$S_\phi^{\rm new}(r) = -\frac{4\pi G r^2 e^{2\Lambda(r)}}{c_{s,\rm eff}^2}\left[\frac{2\beta^2\rho(r)}{M^2 P_{\rm eff}(r)}\left(1 + c_{s,\rm eff}^2\right)\right](\epsilon_{\rm eff}(r) + P_{\rm eff}(r))\Xi(\phi), \tag{A.20}$$

which is the operational form used by the compact-object solver to map the Golden coupling β into a Love-number prediction.

Relativistic contextuality in curved spacetime (AO3).

Beyond static Bell configurations, the archive defines a covariant contextual weight tied to a causal-diamond boundary flux:

$$\rho(\lambda \mid C) \propto \exp\left[-\frac{1}{\hbar_{\rm eff}}\int_{\partial V} n^\mu \partial_\mu \phi[C]\, d\Sigma\right]. \tag{AO.3}$$

Curvature-induced geometric phase (AO4).

For atom interferometers and "Quantum Geometric" tests, the scalar sector induces an extra geometric phase that can be written as

$$\Phi_{\rm geo} = \oint_{\partial\Sigma} A_\mu^{\rm eff}\, dx^\mu \approx \frac{\beta_K}{M^2}\int_\Sigma R_{\mu\nu\rho\sigma}\, e^{\mu\nu}\, dx^\rho \wedge dx^\sigma. \tag{AO.4}$$

Jeans/pressure filtering transfer function (AA.1–AA.2).

To suppress unphysical small-scale baryon clustering (and to implement the "pressure filter" used in the hydrodynamic/IGM consistency module) the archive uses the Jeans scale

$$k_J(a) = \sqrt{\frac{3}{2}}\frac{aH(a)}{c_s(a)}, \tag{AA.1}$$

and the associated smooth filter

$$S_J(k,a) = \exp\left[-\left(\frac{k}{k_J(a)}\right)^2\right]. \tag{AA.2}$$

Scale-dependent growth and baryon power evolution (F.1).

For IGM/Lyα consistency checks the scale-dependent linear growth $D(a,k)$ and its logarithmic rate are defined by

$$f(a,k) \equiv \frac{d\ln D(a,k)}{d\ln a}, \qquad P_{\delta_b}(k,z) = D^2(a,k)\, P_{\delta_b}(k, z_{\rm ini}). \tag{F.1}$$

 doi:10.20944/preprints202512.2427.v1

Smooth pressure filtering and flux-power mapping (F2–F3).

A smooth pressure filter is applied before mapping baryon fluctuations into transmitted flux:

$$k_J(z) \simeq \frac{\sqrt{3}\,aH(z)}{2\,c_s(T_0)}, \qquad S_p(k) = \exp\left[-\left(\frac{k}{k_J}\right)^2\right], \qquad P_{\delta_b} \to S_p(k)\,P_{\delta_b}. \tag{F.2}$$

In the linear FGPA mapping the 3D flux power spectrum is taken as

$$P_F(k,\mu,z) = b_F^2(z)\left[1+\beta_F(z,k)\mu^2\right]^2 P_{\delta_b}(k,z). \tag{F.3}$$

Here $\mu \equiv \hat{k}\cdot\hat{n}$ is the cosine to the line of sight, and b_F, β_F are the effective bias and Kaiser factor used in the pipeline documentation.

5. Laboratory Handoff: the T-Environment Density-Swap Test

The T-Environment experiment is the *replication vehicle*: it turns a one-off network candidate into a controlled laboratory signal by *actively modulating the local density* around a precision sensor. The core prediction is degree-of-freedom-free: a rapid change in $\rho_{\rm env}$ forces a non-adiabatic change in $\tau(\rho_{\rm env})$, producing a mandatory negative chirp and exponential relaxation consistent with the "Sad Trombone" template (Section 2.5). This section is written as a *handoff page*: it tells an independent laboratory *exactly* what to build, what to log, what to run, and what constitutes a pass/fail.

5.1. What Must Be Built

At minimum, the setup must provide:

- A phase-sensitive sensor (SERF-class magnetometer or EDM-cell phase readout) with bandwidth sufficient to resolve τ in the stiff regime.
- A controlled density modulator that can repeatably switch between a *high-density* configuration and a *low-density* (vacuum/void) configuration around the sensor.
- Magnetic shielding and environmental monitoring adequate to apply Platinum-style vetoes.

A concise engineering snapshot is given in Table 11.

5.2. Timing and Invalidation Rules (Hard Stop)

The density swap must be fast compared to the expected τ to avoid adiabatic tracking. The handoff adopts a *hard invalidation rule*: any swap with transit time $\Delta t \geq 50$ ms is *automatically invalid* for MMA–DMF signal claims (the field relaxes before the measurement window). Operational timing and logging requirements are summarised in Table 15.

Table 15. Selected operational requirements for the density-swap (T-Environment) protocol. Any violation of the hard-stop constraints invalidates the run for MMA–DMF claims.

Component	Requirement	Acceptance criteria
Trigger timing	Jitter < 10 μs RMS	timestamp monotonic; commissioning + each run
High-density shield	Thickness ≥ 20 cm	full coverage around sensor path
Transit time	Hard stop < 50 ms	any swap with $\Delta t \geq 50$ ms invalidates run
Minimum log fields	canonical CSV schema	no nulls in critical fields

5.3. Data Acquisition and Logging

Replication requires raw time series stored at ≥ 5 kHz sampling, with:

- monotonic trigger timestamps (sub-10 µs RMS jitter),
- explicit state labels for the density configuration (`HIGH/LOW`),
- synchronous environmental channels (temperature, vibration, local field monitors),

 doi:10.20944/preprints202512.2427.v1

- full metadata: shield geometry, swap actuator parameters, vacuum level, and calibration constants.

The Diamond candidate event summary (Table 8) defines the minimum fields needed to interpret a run as a handoff anchor.

Table 16. Minimum raw-run CSV schema (`data/raw/`) for a single T-Environment trial. Labs should log these fields without nulls; any missing critical field invalidates the run for MMA–DMF claims.

Field	Units / type	Notes
`t_unix_s`	seconds (float)	Monotonic timestamps; sampling $\geq$ 5 kHz.
`state`	enum	`HIGH/LOW` density label (must align with trigger).
`rho_env_gcm3`	g/cm^3	Effective local density for each state (measured/estimated).
`p_torr`	Torr	Vacuum pressure (LOW state) + any residual gas changes.
`B_bias_nT`	nT	Bias field used for Zeeman-discrimination sweeps.
`omega_L_rad_s`	rad/s	Instantaneous Larmor/Ramsey frequency trace (raw).
`temp_C`	°C	Temperature monitor at sensor head.
`vib_g`	g	Vibration / accelerometer channel (systematics veto).
`swap_dt_s`	seconds (float)	Transit time; must satisfy hard stop $<$ 50 ms.
`trigger_id`	string/int	Run identifier; links to config + calibration constants.

5.4. Handoff Bundle (Single-File Delivery; Fixed Directory Layout)

To let independent laboratories replicate the experiment *without re-implementing the analysis from scratch*, the handoff must be delivered as a **single archive file** (e.g. `handoff_tenv.zip`) with a **fixed directory structure**. If the structure is not identical, the replication is not audit-equivalent.

1. Configurations and parameters (`config/`)

- `golden_params.json`: the rigid, immutable theory inputs (e.g. $M = 100$ TeV); *no free knobs*.
- `template_spec.json`: exact template generation rules (chirp sign, $\tau(\rho)$ scaling, gating including Eq. (U.15c)); prevents arbitrary choices.

2. Software artifacts (`scripts/`)

- `matched_filter.py`: reference SNR calculation using density-aware templates.
- `whiten.py`: PSD estimation + whitening.
- `qc_vetoes.py`: Platinum veto logic, hard null trials, and Diamond gating rules.
- `forensic_diamond.py`: end-to-end reference pipeline (recursive HDF5 ingestion across heterogeneous lab schemas, PSD whitening via Welch, matched filtering, and Diamond gating).
- `diamond_network_coherence.py`: reference multi-station coherence validator implementing Eq. (U.21) (density-aware delays and morphology alignment).

3. Datasets (`data/`)

- `injections/*.h5`: "known-good" synthetic injections (negative chirps) used to validate the lab pipeline recovers the expected SNR.
- `cal/`: calibration baselines: `no_swap`, `sham_swap`, and `slow_swap` (must fail by hard-stop rules).
- `raw/`: slot for sensor time series and environmental channels (canonical schema in Table 16).

 doi:10.20944/preprints202512.2427.v1

4. Protocols and reports (`results/`)

- `snr_summary.csv`: canonical output schema (Table 18); must report SNR, fitted τ, chirp sign, veto flags, density metadata.
- `checklist.md`: execution checklist for required control runs and pass/fail gates.
- `run_report.md`: minimal run report template (hardware config, calibration constants, swap timing histograms).

Minimum handoff bundle layout.

```
handoff_tenv/
  README.md
  config/
    golden_params.json
    template_spec.json
  scripts/
    matched_filter.py
    whiten.py
    qc_vetoes.py
    forensic_diamond.py
    diamond_network_coherence.py
  data/
    injections/
    cal/
    raw/
  results/
    snr_summary.csv
    checklist.md
    run_report.md
```

Table 17. Handoff file manifest: minimum artifacts required for an independent T-Environment replication without re-implementing the MMA–DMF pipeline.

Artifact (path)	Purpose / acceptance impact
`config/golden_params.json`	Fixed parameters (degree-of-freedom-free); must match Table 1 exactly.
`config/template_spec.json`	Template rules (chirp sign, $\tau(\rho)$ scaling, and gating such as Eq. (U.15c)); prevents silent choices/tuning.
`scripts/matched_filter.py`	Reference SNR implementation (Eq. (25)) including density-aware templates; must reproduce injection SNR within tolerance.
`scripts/whiten.py`	PSD estimation + whitening used before matched filtering; required for reproducible SNR.
`scripts/qc_vetoes.py`	Platinum vetoes + null trials; required for Diamond status and to reject systematics.
`scripts/forensic_diamond.py`	Forensic reference implementation: robust HDF5 ingestion, Welch-PSD whitening, matched filtering, and QC orchestration; prevents labs from silently re-implementing critical details.
`scripts/diamond_network_coherence.py`	Network-coherence reference code for multi-station validation (Eq. (U.21)); required if the lab participates in GNOME-style coincidence tests.
`data/injections/*.h5`	"Known-good" injection set used to validate that the code path recovers negative chirps at the expected SNR.
`data/cal/`	Control runs: no-swap baseline; sham-swap; slow-swap (must fail the hard-stop).
`data/raw/`	Raw sensor + environmental time series; schema must satisfy Table 16.
`results/snr_summary.csv`	Canonical output: SNR, fitted τ, chirp sign, veto flags, transit-time pass/fail, and density metadata.
`results/checklist.md`	Execution checklist for required control runs and acceptance gates.

 doi:10.20944/preprints202512.2427.v1

Table 18. Canonical output schema (`results/snr_summary.csv`). Labs must produce this table for every run; any missing critical field invalidates the run for MMA–DMF claims.

Field	Type	Meaning
`run_id`	string	Unique run identifier (links to raw + cal + config).
`swap_dt_s`	float	Measured transit time; must satisfy $\Delta t < 50$ ms.
`rho_high_gcm3`	float	HIGH-state effective density.
`rho_low_gcm3`	float	LOW-state effective density.
`snr_peak`	float	Peak matched-filter SNR.
`tau_fit_s`	float	Fitted relaxation time τ (must obey Eq. (18) without retuning).
`chirp_sign`	enum	`NEG` required for pass; `POS` is fail.
`veto_flags`	string	Concatenated QC veto bits (magnetic/thermal/vibration/null-trial).
`verdict`	enum	`PASS/FAIL/FAIL_HARDSTOP`.

5.5. Equation Mapping to the Audited Execution Texts

The latest audit texts make explicit which formulae are *operational* (used in execution) versus *supporting* (consistency scaffolding). In the handoff bundle, the relevant equations are referenced by tag:

- In the "Final Report & Laboratory Handoff" material: Eq. (18) (density–time Rosetta law), Eq. (U.15c) (nuclear saturation gate), and Eq. (U.21) (network coherence statistic).
- In the "Diamond & Science Run 5" execution report: Eq. (10.31) (cross-covariance term) and the practical detection filters implementing Eq. (18) and Eq. (U.21) for the Event 4328 candidate.

5.6. Acceptance Criteria (Degree-of-Freedom-Free)

A run is a MMA-DMF *pass* only if: (i) the recovered chirp sign is negative ($\frac{d\omega}{dt} < 0$); (ii) the fitted τ scales with ρ_{env} according to Eq. (18) with *no* re-tuning of α; (iii) null trials (scrambled phase/off-band) suppress the SNR as specified by the Platinum veto suite; and (iv) the pipeline recovers the provided injections at the expected SNR. These gates are intentionally non-negotiable: if they fail, the model fails.

6. Discussion

The MMA-DMF archive proposes a coherent program that ties cosmological consistency, microphysical CP dynamics, and precision-coherence phenomenology into a single operational framework. The principal interpretive claim is that EDM constraints should be applied to *transient spectra* rather than DC offsets, because density-dependent relaxation naturally suppresses time averages at late times. This shifts experimental emphasis toward (i) reanalysis of archived precision datasets without static detrending and (ii) dedicated density-swap experiments engineered to isolate density dependence. The Gold/Platinum/Diamond hierarchy makes explicit that model validation is not purely about obtaining a best-fit parameter set; rather it is about establishing a signal model whose morphology (negative chirp) and environmental scaling ($\tau \propto \rho^{-1/2}$) are discriminative. The use of smootherstep gates, strict FDT closure, and spectral positivity tests addresses a common failure mode in stochastic-scalar simulations: spurious long-duration drift from numerical artifacts. The unit-consistency test further anchors the physical plausibility of the density-to-frequency mapping, ensuring that the same core equations can be used across FRB-like and laboratory-like regimes without dimensional ambiguity. The main limitations are operational. The density-swap laboratory protocol requires strict timing control (hard-stop transit times) and comprehensive logging, and its validity hinges on entering the intended stiff/soft regimes without adiabatic relaxation during transitions. Similarly, network-coherence claims depend on properly modeling density-dependent delays and on prohibiting static filtering that could remove the target low-frequency structure. These limitations are not fatal, but they define the engineering and analysis constraints required for a definitive test.

 doi:10.20944/preprints202512.2427.v1

7. Conclusions

The MMA-DMF EDM program, as represented by the audited archive, is intended to be executed as a *rigid, degree-of-freedom-free* pipeline: the Golden parameter set is fixed, no per-dataset knobs are introduced, and all claims reduce to falsifiable protocol outcomes. Using the full provided archive, we have produced a unified scientific manuscript for the MMA-DMF CP/EDM program. The theoretical core is a chronology mechanism that reconciles early-universe CP activity with late-time EDM null results via geometric locking, thermal kicking, and density-dependent screening. The operational core is a density-controlled relaxation transient that manifests as a negative chirp in precision-coherence measurements, motivating matched filtering with dynamically generated templates rather than static detrending. The archive tests establish: (i) thermodynamic stability via strict exponential-kernel FDT closure and spectral positivity; (ii) a methodology for false-positive suppression using injections and null-phase trials; (iii) a unit-consistent mapping from density to effective mass/frequency; and (iv) an executable Diamond pipeline specification with mandatory dynamic filtering and logging constraints. The decisive next step is experimental: implement the T-Environment density-swap laboratory protocol under the stated hard-stop timing and logging requirements, and reanalyze archived nEDM/EDM/co-magnetometer drift channels using the density-dependent matched-filter templates defined here.

7.1. Audit-Derived Conclusions Beyond the Core EDM Narrative

The audited technical notes include several conclusions that are not strictly required to *run* the EDM pipeline, but materially affect how legacy null results are interpreted, how the fifth-force hypothesis is operationally framed, and what constitutes a decisive next experimental step.

1. **The detrending fallacy (why others can fail).** Audit notes argue that standard "slow-drift removal" in frontier EDM analyses (e.g. high-pass filtering or polynomial detrending) can erase precisely the predicted low-frequency, density-driven *negative-chirp* transient. In that reading, decades of "instrumental drift rejection" may have been systematically discarding the sector's target morphology rather than cleaning it.
2. **Status of the fifth force: "rejected noise".** The audit conclusion is that static analyses are largely blind to a density-dependent relaxation time $\tau(\rho)$. Consequently, non-Gaussian "glitches" and slow, environment-linked residuals that are usually classified as nuisance structure are treated here as the *search space* where a geometric fifth-force signature would live.
3. **Popperian vulnerability as rigor.** Audit notes emphasize that the "zero-parameter policy" (fixed $M = 100\,\mathrm{TeV}$ and fixed Golden inputs) is intentionally epistemically vulnerable: the program is *designed to be maximally falsifiable*. If the density-swap protocol and reanalyses do not reproduce the predicted scaling and morphology, the model is not rescued by retuning energy scales.
4. **Thermodynamic unification: screening and stability.** Audit logs highlight that the same mathematical structures used to implement screening (gates that suppress couplings in dense environments) also control suppression of unphysical "scalar heating" in the stochastic dynamics. In this framing, vacuum stability and macroscopic screening are two manifestations of the same geometric "impedance" encoded by the kernel/gating architecture.
5. **"Evidence" versus "discovery": the Event 4328 threshold.** Execution notes treat the $\sim 4.2\sigma$ candidate (Event 4328) as *evidence*, not discovery; a conventional discovery bar (5σ) is explicitly not met. The dominant uncertainty is attributed to imperfect environmental density knowledge (e.g. geologic Hayward-density proxies), which makes dedicated T-Environment hardware *mandatory* rather than optional for a definitive claim.
6. **Roadmap to a deeper theory (next steps).** The handoff material closes with a strategic statement: if rigidity of q_f and M survives laboratory and archival tests, the next milestone is a microphysical derivation of the geometric charges from topology, including an explicit connection between the Higgs sector and the MMA-DMF geometric scaffolding (a "ToE"-oriented program).

 doi:10.20944/preprints202512.2427.v1

7.2. Replication Constraints and Falsifiability Conditions (Audit-Derived)

For completeness, we summarize several replication constraints and falsifiability conditions stated in the audit TXT logs. The statements below are paraphrased from those logs to fit a preprint style; the technical requirements and acceptance logic are unchanged.

1. **Replication mandate: controlled T-Environment driving is required.** In the audits, the density-swap hardware is treated as required to move from an evidence-level ($\sim 4.2\sigma$) candidate toward a discovery-grade ($\geq 5\sigma$) test. Operationally, the point is to enable on-demand driving of the density dependence rather than relying on rare stochastic astrophysical triggers.
2. **Scope of existing static analyses: prior pipelines are not a decisive test.** The audit position is that prior datasets do not constitute a decisive fifth-force test under static, axion-like filtering assumptions. The audits argue that legacy pipelines classified the relevant morphology as "glitches" or "non-Gaussian noise" precisely because they were blind to $\tau(\rho)$-driven variability.
3. **Hard invalidation mode: the transit-time limit is a binary validity criterion.** The manuscript lists a hard-stop transit time ($< 50\,\mathrm{ms}$) as an engineering specification; the audits treat it as a binary validity criterion. If the shuttle motion is slower, adiabatic adjustment can occur, the field can relax before readout, and the density-swap test is invalidated by construction. The audits note that apparent "null" outcomes can therefore arise from mechanical/temporal failure modes, independent of the underlying hypothesis.
4. **Fixed-parameter falsifiability: no retuning of M or Golden inputs.** The fixed $M = 100\,\mathrm{TeV}$ policy is presented academically as precision; the audits frame it as deliberate epistemic vulnerability. There are no parameters to absorb disagreement: if the predicted scaling and morphology fail under the defined protocol, the hypothesis is not retuned; it is treated as falsified under the fixed-parameter policy.
5. **The flavor-charge blind spot: the program is operationally closed, ontologically incomplete.** The audits explicitly acknowledge that q_f and M remain locked but still treated as topological inputs. The handoff concludes that the project is not "complete" until the microphysical origin of these charges is derived (including an explicit Higgs-sector connection), i.e. the ToE-oriented next step.
6. **"Trench engineering" details that matter.** The TXT notes include bench-level directives that rarely appear in polished manuscripts: material choices (e.g. ferrite vs. mu-metal) to suppress eddy-current effects that can mimic scalar drifts, and shielding design details (e.g. ventilation/relief features) to avoid creating an unintended "scalar Faraday cage". These are treated as practical failure modes, not optional optimizations.

Reproducibility requires public release of the digital handoff bundle.

The model's "zero-parameter" posture only has scientific force if independent groups can run the *same* pipeline against their own data. Accordingly, replication should *not* depend on private audit archives. A minimal public release must include: (i) the fixed parameter file `config/golden\_params.json` (including $M \simeq 100$ TeV and the geometric charge spectrum q_f); (ii) the template-generation rules `config/template\_spec.json` (chirp sign, $\tau(\rho)$ scaling, and gating choices); (iii) the reference analysis scripts (matched filtering, whitening/PSD estimation, and QC veto logic), including the forensic and network-coherence modules; and (iv) benchmark datasets for validation (reference injections and "hard null" trials demonstrating SNR < 1.5). Without an archival link/DOI to these artifacts, the work risks being read as "trust the archive" rather than a falsifiable protocol.

7.3. Forensic Code, Trench Engineering, and Raw Benchmarks (Audit-Only Operational Directives)

The manuscript consolidates the physics and the *external* replication protocol, but the audited TXT record is explicit that successful independent replication requires shipping more than equations: it requires the exact operational code paths, the failure genealogy, and the non-negotiable engineering

 doi:10.20944/preprints202512.2427.v1

constraints that prevent silent "pipeline drift". The following items are treated in the audits as part of the **minimum deliverable** for Diamond-grade replication (Audit TXT refs in parentheses).

1. **Forensic source code (the operational brain).** The audits stress that the decisive logic lives in the executable Python reference implementations (e.g. the Diamond coherence driver and network-coherence validator), not in the prose description of Eqs. (U.21) and the matched-filter statistic.
   - **Hierarchical HDF5 ingestion.** The audited code includes recursive HDF5 tree navigation (via `h5py` traversal) so that heterogeneous lab files can be ingested without hard-coding dataset names, locating channels such as `/Station1/MagData` or `/RawData/Bfield` across independent lab conventions (e.g. Berkeley, Hayward, Mainz). (Audit TXT 1–3)
   - **PSD whitening (Welch).** The audits do not merely recommend whitening; they ship the specific PSD-estimation and $1/f$ inversion procedure (Welch-style segment averaging) used to prevent the *negative-chirp* "Sad Trombone" transient from being misclassified as thermal drift. (Audit TXT 9)
2. **Failure genealogy (why earlier pipelines failed).** The audits preserve "forensic" failure logs that explain *how* null outcomes can be produced mechanically or numerically even when the morphology is present.
   - **Unit underflow.** A prior configuration that expressed drifts in GHz/ms caused numerical underflow/rounding so that physically small but nonzero drifts were reported as exactly 0.0, including in magnetar-like cases. (Audit TXT 15)
   - **Scale safety directive.** The audits explicitly note that drifts of order 5×10^{-8} GHz/ms can truncate to zero in typical pipelines, motivating a hard directive to report in MHz/ms (or equivalent) as a safety rule, not a stylistic preference. (Audit TXT 18)
3. **Search parameters for multimessenger triggers (LIGO/Virgo).** The audits include concrete, operator-facing search-window choices for real-world event association, beyond the generic "delay modeling" discussion.
   - **Correlation window.** Use a dedicated search window of $\pm 500\,\mathrm{s}$ around confirmed LIGO/Virgo events when scanning for scalar precursors/"dark series" in network data products. (Audit TXT 21)
   - **Velocity consistency.** Enforce that the inferred wall/feature velocity vector $\vec{v}$ is consistent with a galactic-domain-wall crossing scale, $v \sim 300\,\mathrm{km\,s^{-1}}$, when mapping station delays and density-dependent morphologies. (Audit TXT 22)
4. **Strategic "ToE" roadmap (Next Steps).** The audits are explicit that the current program is operationally closed but ontologically incomplete: it locks q_f and M as topological inputs while deferring their microphysical origin.
   - **Named next project.** The audited handoff identifies the next mandated theory deliverable as "From Higgs Fields to Geometry: The Geometric Origin of Standard Model Masses in the MMA–DMF Framework". (Audit TXT 23–24)
   - **Incompleteness statement.** The framework remains "ontologically incomplete" until the flavor charges q_f are derived microphysically (Higgs-sector linkage), rather than treated as externally provided topological inputs. (Audit TXT 23)
5. **Administrative directive and geological uncertainty.** The audits attach the practical conclusion to the evidence/discovery threshold: the current candidate is limited by geological density estimation uncertainty, and the only path to $\geq 5\sigma$ is controlled density driving.
   - **Hayward-density uncertainty.** The audits explicitly attribute the dominant uncertainty to the fact that the relevant "Hayward density" is presently an estimate rather than a hardware-controlled variable. (Audit TXT 28)

 doi:10.20944/preprints202512.2427.v1

- **Execution directive.** The handoff material includes an internal execution directive (dated 2025-12-24) to build the pneumatic density-swap shuttle promptly, rather than waiting for another random cosmic event, because controlled on-demand driving is required to move from evidence toward discovery-grade significance. (Audit TXT 28–29)

Author Contributions: Conceptualization P.B.; System Conceptualization, H. O.; All authors have read and agreed to the published version of the manuscript."

Funding: This research received no external funding.

Institutional Review Board Statement: There was no need for an Institutional Review Board.

Data Availability Statement: All artefacts required for independent replication are provided as Supplementary Material S1: `MMA_DMF_HandoffBundle.zip`. This bundle contains the fixed parameter JSONs, template specification, reference analysis scripts (PSD whitening, matched filtering, QC veto logic, and HDF5 ingestion helpers), and minimal benchmark inputs/output schema.

Conflicts of Interest: The author declares no conflict of interest.

Code Availability Statement: Reference implementations and the replication bundle are provided as Supplementary Material S1: `MMA_DMF_HandoffBundle.zip`. The scripts are intended as a transparent baseline; laboratories may re-implement the pipeline, but results should be cross-checked against the reference outputs using the supplied benchmark injection(s) and QC null-trial criteria.

References

1. Medical College of Wisconsin, Department of Biostatistics. *Computing FMRI Activations: Coefficients and t-Statistics by Detrending and Multiple Regression*. Technical Report TR039, accessed December 23, 2025. https://www.mcw.edu/-/media/MCW/Departments/Biostatistics/tr039.pdf
2. Doyle Group (Harvard). *ACME Precision Measurement of the Electron Electric Dipole Moment (EDM)*. Accessed December 23, 2025. https://jdoyle.hsites.harvard.edu/tho-electron-edm
3. Liu Lab (UIUC). *nEDM experiments*. Accessed December 23, 2025. https://ultracold.web.illinois.edu/nEDM
4. Preprints.org. *Resolution of the Hubble Tension by a Reversible Fractal Cosmology: The Ultimate Black Hole Framework*. Accessed December 24, 2025. https://www.preprints.org/manuscript/202511.0331
5. CERN Courier. *The Hubble tension*. Accessed December 24, 2025. https://cerncourier.com/a/the-hubble-tension/
6. arXiv:2501.08391. *Multi-axion like description of the dark sector in light of the Hubble and σ_8 tensions*. Accessed December 24, 2025. https://arxiv.org/abs/2501.08391
7. V. Andreev *et al.* (ACME Collaboration). *Improved limit on the electric dipole moment of the electron*. Nature **562**, 355–360 (2018).
8. B. Graner, Y. Chen, E. G. Lindahl, and B. R. Heckel. *Reduced Limit on the Permanent Electric Dipole Moment of ^{199}Hg*. Phys. Rev. Lett. **116**, 161601 (2016).
9. C. Abel *et al.* (nEDM Collaboration). *Measurement of the permanent electric dipole moment of the neutron*. Phys. Rev. Lett. **124**, 081803 (2020). doi:10.1103/PhysRevLett.124.081803; arXiv:2001.11966.
10. W. B. Cairncross *et al. Precision measurement of the electron's electric dipole moment using trapped molecular ions*. Phys. Rev. Lett. **119**, 153001 (2017). doi:10.1103/PhysRevLett.119.153001.